

# Towards Optimized Carbon Nanotubes (CNTs) Reinforced Polyetherimide (PEI) 3D Printed Structures: A Comparative Study on Testing Standards

Alptekin Yıldız<sup>a,e</sup>, Uğur Emanetoğlu<sup>b,e</sup>, Elif Ozden Yenigun<sup>c,e</sup>, Hulya Cebeci<sup>d,e,\*</sup>

<sup>a</sup>Aviation Institute, Istanbul Technical University, Istanbul, 34469, Turkey

<sup>b</sup>Polymer Science and Technology, Istanbul Technical University, Istanbul, 34469, Turkey

<sup>c</sup>School of Design, Textiles, Royal College of Art, London, SW7 2EU, United Kingdom

<sup>d</sup>Department of Aeronautical Engineering, Istanbul Technical University, Istanbul, 34469, Turkey

<sup>e</sup>Aerospace Research Center, Istanbul Technical University, Istanbul, 34469, Turkey

---

## Abstract

Tailoring the properties of high-performance polymers through reinforcing will bring multifunctionality and expand their use in additive manufacturing (AM). However, machine and material-based challenges exist, eventually resulting in low-quality end products. When expensive polymers are considered, it is still challenging to tailor their properties and print them for high-quality multifunctional structures. Here, polymer composites of polyetherimide (PEI) and carbon nanotubes (CNTs) with varying CNT weight fractions are produced in filament form by melt-processing. Neat PEI, 1 wt.% and 3 wt.% CNTs/PEI are additively manufactured in two different raster orientations (*Rectilinear* and *Concentric*), and two most proposed testing geometries, ASTM D638 and D3039. Through effective melt-processing, CNT-reinforced PEI filaments were achieved, printing parameters and testing protocols were discussed. As a result, ASTM D3039 showed superior coherence with filaments' mechanical properties. Moreover, based on failure modes, ASTM D3039 provided better compatibility to AM, owing to its simple rectangular form yielding well-adhered layers.

**Keywords:** Carbon nanotubes, PEI nanocomposite, Additive Manufacturing, Mechanical properties and standards, Multifunctionality

---

## 1. Introduction

Design flexibility in composites is one critical aspect considered for demanding fields such as aerospace. Since carbon fiber reinforced plastics (CFRPs) have been the major player in structural applications, several researchers considered many novel approaches, especially combining novel materials and manufacturing technologies, as a critical platform to push the boundaries and change the paradigm for the future of structures. High-performance thermoplastics such as polyetherimide (PEI), polyether ether ketone (PEEK), are keen to replace CFRPs; however, they are still far from the reality due to the lack of comparable mechanical properties with CFRPs. Hence, one particular strategy can be strengthening mechanisms of these polymers using nanoparticle reinforcements such as carbon nanotubes (CNTs), graphene, hexagonal boron nitride (h-BN), and aluminum nitride (AlN) that will also bring multifunctionality as an advantage. Although reinforcement brings tunability, additive manufacturing (AM) can be the novel platform for these materials to create complex structures with enhanced mechanical characteristics for advanced applications.

Thermoplastics that are processable by fused filament fabrication (FFF) as an AM methodology come in a wide variety and fulfill the needs of numerous applications such as rapid prototyping, rapid tooling/moulding, direct formed usable part, nano-/micro-manufacturing, and biomanufacturing [1]. PEI and PEEK are applicable for these purposes and are referred to as high-performance polymers that can operate at high temperatures with their superior durability

---

\*Corresponding authors

Email address: hulya.cebeci@itu.edu.tr (Hulya Cebeci)

to their engineering-grade counterparts. PEI is an amorphous polymer with a glass transition temperature ( $T_g$ ) of 217 °C and a high ultimate tensile strength (UTS) of 101 MPa. [2, 3]. These properties, combined with their low flammability and density along with high chemical resistance, justify PEI as an excellent material to replace high-density, corrosion-prone [4, 5] metal parts in the final products, especially for the aerospace industry [6]. Moreover, FFF is sought for processing multifunctional polymer composites with nano- and micro-scale fillers, including CNTs, graphene nano-platelets (GNP), h-BN, and CFs. These reinforcements provide a wide range of mechanical strength and electrical and thermal conductivity to the base polymer [5, 7]. These reinforcing strategies indicate that FFF can be one step ahead of conventional manufacturing processes by adding tunability to aerospace components such as electrical and thermal conductivity combined with lightweight and high strength.

Among several reinforcements, CNTs can be employed in polymers to obtain superior mechanical and thermal properties and electrical conductivity for achieving these multifunctionalities [5, 8–16]. Yang et al. have reported that the tensile strength of 3D printed PLA/CNTs composites increased proportionally with CNTs content, which is capped at a 64.12% increase with a 6 wt.% CNTs addition. However, it is unclear if this increase is the maximum achievable value since no further test has been performed with CNTs contents higher than 6 wt.% [8]. Siochi et al. obtained CNTs/PEI composites by melt compounding, and the UTS was increased from 91 MPa to 96 MPa for 0.3 wt.% CNTs/PEI composite compared to that of neat PEI. Furthermore, for 1 wt.% CNTs/PEEK composite the UTS have reported as 101 MPa for filament-like rods which are 1 mm in diameter [9]. Although reinforcing PEEK and PEI with nanomaterials brings mechanical advantages, it is still unclear how much the improvement is realistically achievable due to the effects of the printing process and testing method variations on the overall mechanical characteristics. Hence, a careful and detailed mechanical property investigation should be performed if AM will be considered as a replacement to conventional manufacturing methods or even be used in conjunction with them.

Nowadays, AM's unique feature to produce complex geometries that traditional manufacturing systems are not capable of has rendered it a unique method with tailorable characteristics. However, due to the production process, where semi-elliptical strings of filaments are laid on a flat surface, FFF results with porous structures, especially between the interfaces of the deposited filament, thus distinguishing FFF from injection molding. Even though the porosity caused by the process can be reduced by optimizing the printing parameters, this phenomenon is nearly unavoidable. Moreover, interdiffusion between neighboring laid material plays a vital role in the mechanical results. Along with the porosity and limited interdiffusion, the layered nature of FFF results in a decrease in mechanical properties. Several studies have inspected and verified these widely studied phenomena [3, 17–26]. Chuang et al. performed AM studies for developing aircraft engine components from Ultem 9085, Ultem 1000 and carbon fiber (CF) reinforced Ultem 1000 resins. The mechanical properties revealed that printed parts presented an 87% and 64% reduction in strength and modulus, respectively. The main reason for this was the porosity and lack of limited adhesion between layers [18]. Moreover, Chacón et al. studied the effect of printing parameters on the overall mechanical properties of printed specimens when a continuous fiber reinforcement is present in PLA and ABS [19]. Therefore, a combined effort to enhance the properties of high-performance polymers by fillers and tuning the process parameters of printing can bring a successful material-process combination to achieve reliable and improved mechanical characteristics. Through this effort, it is also valuable to interpret proper testing methodologies to identify the effect of either printing parameters and/or reinforcing strategies for establishing final products.

Mechanical testing of additively manufactured parts is dominantly conducted by the ASTM D638 method designed for traditional manufacturing methods [17, 27, 28]. ASTM D638 tensile coupons contain a curved geometry between the gage and grips. This feature prevents stress concentration on the gage while tensile testing. Nevertheless, FFF systems build a layer through linear displacements of the nozzle on the x and y axes, approximating these linear displacements into a radiused curve leaves porosity, especially on the interface between the shell and the infill. Thus, resulting in the radiused feature to cause precisely the opposite of what it should prohibit, stress concentrations are accumulated around the gage. This implies that AM encounters the porosity and lack of interdiffusion difficulties and appropriate mechanical testing of its products. Therefore, a tensile test standard as ASTM D3039 designed for polymer matrix composite materials is also proposed by numerous researchers for 3D printed parts and pieces [3, 21, 29–33]. This rectangular prism geometry provides more reliable tensile data consistent with the failure criterion [29]. Rankouhi et al. have stated that stress concentrations occur mainly at the very points where raster discretization presents, mainly at the interface of infill and the outer shell. They have concluded that using ASTM D3039 tensile test coupons would reduce this negative effect [21]. Zaldivar *et al.* have drawn attention to the anisotropic nature, thus to the composite behavior of FFF products, and noted that utilizing ASTM D3039 would evaluate the mechanical

properties more effectively [34]. Kay *et al.* pointed out that Young's modulus is an essential feature for the designs to prevent failures of produced components. It is further concluded that ASTM D3039 specimens result in more precise values for determining the Young's modulus than ASTM D638 Type I [35]. Additionally, Somireddy *et al.* also have conducted tensile testing of 3D printed parts within the scope of ASTM D3039 with a motivation of laminate composite behavior of FFF processed parts. It was clearly stated that their experimental results were in harmony with analytical modeling and finite element analysis; thus, laminate mechanics may be attributed as a better approach for the mechanical characterization of 3D printing where applicable [31]. Furthermore, Miller *et al.* have conducted extensive research comparing ASTM D638 and ASTM D3039 methods. Their work suggests that although ASTM D638 specimens yield more accurate results for UTS, ASTM D3039 has a substantial advantage over D638 on failure acceptance criteria thus, giving consistent and reliable findings on mechanical tests [29]. Hence, the realistic evaluation of mechanical properties can be performed independent of the production methodology and this discussion is noteworthy for AM to develop end-user applications compared to prototyping when industrially scalable systems such as big area additive manufacturing (BAAM) are also considered. Especially for reinforced composites with changing viscosities due to the addition of fillers, these AM processes with a single screw extrusion system are found to be assertive instead of a heated chamber in a conventional FFF systems[36–38].

In this study, initially, we attempt to engineer CNTs reinforced PEI filaments by melt-processing to reveal the effect of reinforcement on the overall properties of composite filaments, followed by a complete discussion to print the CNTs/PEI filaments with optimized processing parameters and proper testing protocols. Since the challenge lies in identifying the printing parameters when reinforced polymers are being considered, rheology and thermal characterizations were used to evaluate how the CNTs/PEI filaments viscosity and thermal degradation changes at different processing parameters and various filler loadings. TGA showed that it was depicted that CNTs addition to PEI increased the thermal stability from 524 °C to 539 °C and 537 °C for 1, and 3 wt.% CNTs, respectively. The complex viscosities and shear thinning of CNTs/PEI composite filaments were increased at higher filler loadings which were attributed to an additional pressure required during the extrusion of the FFF system for a better printing efficiency especially when considered for BAAM related processes. All neat and CNTs/PEI composite filaments were also tested under tension to identify the strength and stiffness after extrusion when CNTs reinforcements were considered. The results indicated that adding CNTs to PEI exhibited a 5% increment in UTS compared to the neat polymer, similar to literature findings. Since the mechanical properties of tensile coupons are highly affected by the printing parameters, neat, 1, and 3 wt.% CNTs/PEI filaments were studied by printing a single layer to identify the effective nozzle temperature from 360-390 °C. After revealing the effect of CNTs on both process and printing parameters, the printed specimens were tested with ASTM D638 Type IV and ASTM D3039 for a *Rectilinear* and *Concentric* pattern to correlate the difference that may arise from the testing protocol. The lower standard deviation of UTS of ASTM D3039 samples has indicated that this test standard can yield more reliable mechanical results than ASTM D638. The results presented failures mostly in multiple areas for failure modes of D638 and D3039 tested FFF specimens. Although D638 failure types were dominated at the radiused region leading to an unsuccessful testing process, ASTM3039 presented lateral gage region dominated multiple areas failures representing the capability with the low standard deviation in strength.

## 2. Materials and Methods

Polyetherimide (PEI) granules were obtained from Sabic (ULTEM 1010,  $C_{37}H_{24}O_6N_2$ , Density: 1.27 g/cm<sup>3</sup>, MW: 592 g/mol, glass transition temperature ( $T_g$ ): 217 °C). CNTs were delivered by Nanokomp (industrial-scale multi-walled CNTs with purity above 90%, average diameter: 9.5 nm, length: 1.5–2  $\mu$ m). Both chemicals were utilized without any further purification.

Similar to the previous studies [7], all filaments were fabricated by a custom-made extrusion assembly (Kökbir Import&Export), specifically designed for high-performance thermoplastics. The extrusion unit is composed of a twin-screw and single-screw extruder, and all two screws have a diameter (D) of 12 mm and length (L) of 264 mm, which corresponds to an L/D ratio of 22. The detailed extruder and process information is given in the earlier studies [7].

Neat PEI filament fabrication was performed by feeding the twin-screw extruder with neat PEI granules dried in a convection oven (Nüve KD 400) at 150 °C for eight hours before processing barrel temperature of 310-360 °C from the hopper to the die. 1 and 3 wt.% CNTs/PEI filament fabrications were performed through feeding the CNTs

to PEI from a side-feeder revealing an effective melt-processing through optimized extrusion parameters to avoid agglomerations. CNTs/PEI composites are produced by 5 cycles in the twin-screw extruder to obtain homogenous distribution and dispersion [7]. Although the mechanical properties of the neat PEI polymer may result a slight decrease upon recycling, a higher cycle number during melt compounding was led to a well-distributed CNTs which compensated the decrease in neat PEI as presented in filament tensile testing. An illustration of melt-processing for composite filament fabrication and produced filaments of neat PEI and 3 wt.% CNTs/PEI with a nominal diameter of 1.75 mm can be seen in Fig. 1.

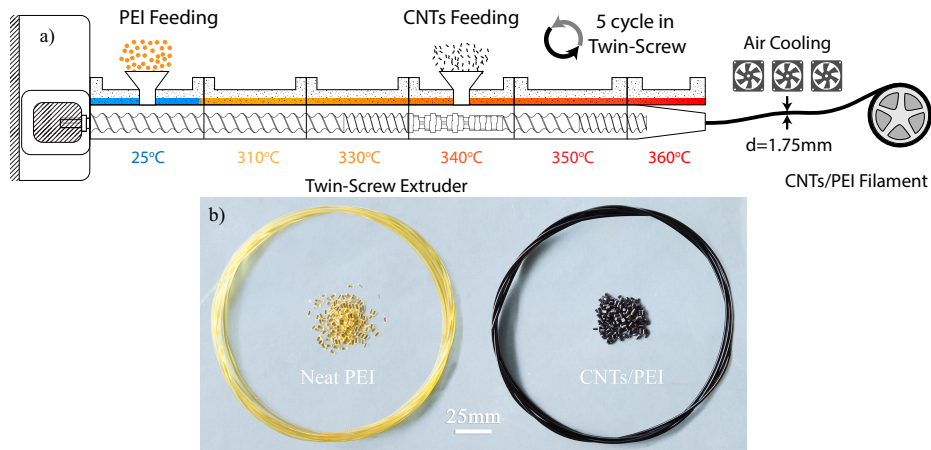


Figure 1: (a) Schematics of melt-processing by extrusion for granules and filament production and (b) granules and filaments of neat PEI and 3 wt.% CNTs/PEI.

### 2.1. Thermal and Rheological Characterizations

Thermogravimetric analysis (TGA) was performed using a TA Instrument TGA 55 thermogravimetric analyzer. The granule samples of filaments were heated to 800 °C from 30 °C with a heating rate of 10 °C/min under a nitrogen ( $N_2$ ) atmosphere. Difference thermogravimetry (DTG) curves were plotted from the first derivative of TGA weight loss raw data for the temperature to assess the thermal stability of CNTs/PEI composites. The peak points of these DTG thermographs were determined for each sample's thermal decomposition temperatures ( $T_d$ ).

All rheological measurements of the neat PEI and CNTs/PEI composites were carried out using a TA Instruments Discovery HR-2 equipped with 25 mm plate geometry under  $N_2$  atmosphere. Before each frequency sweep test, the samples were positioned between the preheated plates at 360 °C and held for five minutes to transform the granules into the melt phase. Storage modulus, loss modulus, and complex viscosity were reported as a function of the angular frequency range between 0.05 and 100 Hz (0.31 and 628 rad/s).

### 2.2. Electrical and Mechanical Characterizations

The electrical conductivity was characterized at room temperature by a four-point probe device, FPP 470 (Entek Electronics, Turkey). After cutting 2.5 cm length, the specimens were polished on one side using a sequence of grits (400, 800, 1200, and 2500) to a thickness of around 0.85 mm in preparation for measurement. The average value of five samples was used in the electrical conductivity equation with geometric correlation factors to calculate filaments' conductivity [7, 39].

### 2.3. Tensile testing of neat and CNTs reinforced filaments

Tensile testing of neat and CNTs reinforced PEI filaments was performed at room temperature using a Shimadzu AGS-X 50 kN testing machine equipped with a load cell of 1 kN capacity single-bollard, self-tightening type grips (Fig. 5, Route-1). The tensile properties of neat PEI, 1 and 3 wt.% CNTs/PEI filaments, such as their ultimate strength, fracture strength, and tensile modulus, were determined at a crosshead speed of 5 mm/min, and each test was repeated at least 8 times. In accordance with ASTM 3822D, 105 cm long specimens with 20 cm gauge length were tested.

#### 2.4. Additive manufacturing of coupon specimens by a custom-built 3D printer and mechanical characterizations

Despite the abundant availability of FFF printers, very few can print at high temperatures needed for PEI and PEEK as high-performance engineering polymers. Especially when AM-enabled composites are considered, the filaments manufactured by reinforcing nano- and/or micro- fillers require customized instruments to tune the microstructures and realize their superior characteristics. Hence, an FFF printer (named as ARC-Pegasus) was designed and built to conduct the printing studies here, as presented in Fig. 2. ARC-Pegasus can print high-temperature materials, owing to its full metal design. The nozzle (Dyze Design Tungsten Carbide Nozzle) can reach up to 500 °C, whereas the print bed enables high-performance printing materials prone to warping, with its temperature rating up to 200 °C. Furthermore, to process these materials, a thermal chamber was also built which can operate up to 90 °C, with a particular role in decreasing the thermal stresses on the products during printing, thus preventing warping. As mentioned above, the full-metal design of ARC-Pegasus entirely consists of materials that are resistant to high temperatures. ARC-Pegasus can process materials, including but not limited to PEI, PEEK, PLA, ABS, TPU, NYLON, and PC.

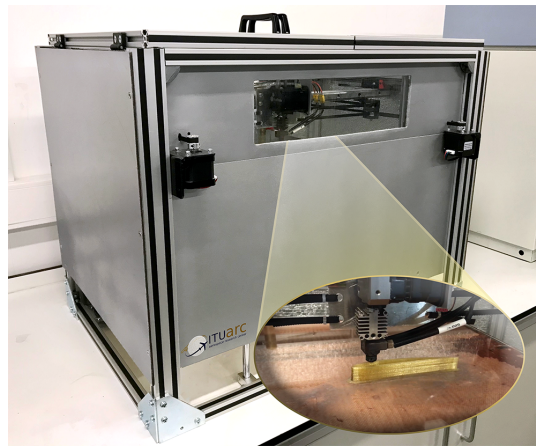


Figure 2: Custom-built high-performance FFF Printer named as ARC-Pegasus with an inset of exemplary work on printing PEI at an optimized protocol with high quality.

In Fig. 3, the schematics of ASTM D638 Type IV and ASTM D3039 tensile test specimens were presented with the required dimensions for further analysis on mechanical testing of printed parts.

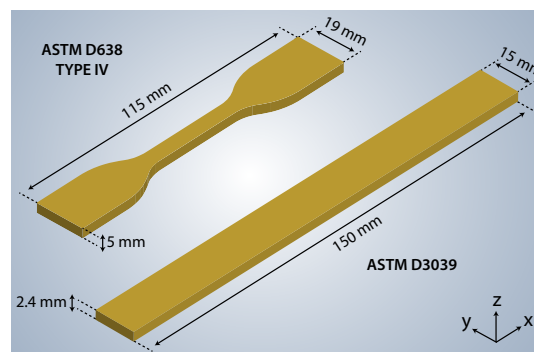


Figure 3: ASTM D638 Type IV and ASTM D3039 specimen dimensions.

Neat PEI, 1 wt.% and 3 wt.% CNTs/PEI samples were all printed with two basic infill patterns: *Rectilinear* and *Concentric*. The difference between these patterns is the angles of printed lines with respect to the specimen edges. While the lines that belong to the *Rectilinear* pattern have an angle of 45° to edge, the lines that belong to the *Concentric* pattern have an angle of 0° to edge, in other words, parallel to the edge. All specimens were printed with 3 outer shells and 100% infill rate to provide structural integrity without any support structure. The nozzle diameter

was 0.4 mm with a layer height of 0.24 mm. Nozzle temperatures were also investigated as a printing parameter and the effective ones were determined upon the CNTs concentration as 375 °C, 380 °C, and 385 °C for neat PEI, 1 wt.%, and 3 wt.% CNTs/PEI filaments, respectively. The printing temperature is varied and will further be discussed in the results section. Additionally, the printing bed temperature was 150 °C with a chamber temperature of 90 °C. In Fig. 4, *Rectilinear* and *Concentric* ASTM D638 Type IV and D3039 printed coupon specimens with directions of printing and routes were shown.

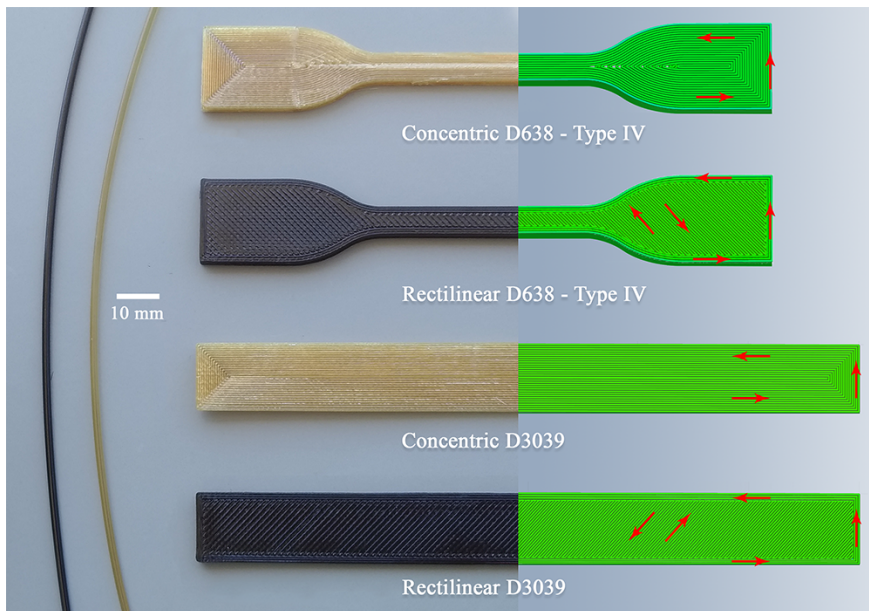


Figure 4: Representative 3D printed specimens for ASTM D638 Type IV and D3039 as *Rectilinear* and *Concentric* patterns showing neat PEI and 1 wt. % CNTs/PEI with the printing directions.

Additively manufactured ASTM D638 Type IV and ASTM D3039 specimens were also tested by Shimadzu AGS-X with a load cell of 50 kN capacity in tensile mode. A stroke speed of 2 mm/min was applied to perform the tensile testing of ASTM D3039 specimens. Fig. 5 presents the road map of the mechanical test in this study for both neat and CNTs/PEI filaments and printed samples.

### 3. Results and Discussion

Thermal decomposition temperature ( $T_d$ ) defines the breaking down of chemical bonds through heating and defines clear information on the thermal stability determined from DTG's peak demonstrated in Fig. 6. For PEI, since aromatic imide units of PEI provide higher thermal stability and flexible ether linkages result in processibility the degradation temperatures close to 500 °C yield to main chain scissioning followed by carbonization. The results showed no significant change in mass up to 500 °C for all materials, implying that additives were not used in the melt compounding process [40]. Onset temperatures of the neat PEI, 1 wt.% CNTs/PEI and 3 wt.% CNTs/PEI were 510.0 °C, 525.7 °C, and 524.8 °C, respectively. The increasing trend for onset temperatures through adding CNTs enhanced the thermal stability of CNTs/PEI composites. Additionally,  $T_d$  of the materials were 523.2 °C, 541.0 °C and 538.8 °C for 15 wt.%; 533.2 °C, 561.6 °C, and 551.8 °C for 25 wt.% decompositions, further revealing the increase as mentioned earlier in thermal stability. The maximum decomposition occurred at 524 °C, 539 °C, and 537 °C for neat, 1, and 3 wt.% CNTs/PEI, respectively. However, a two-step decomposition was observed since PEI has an aromatic group (phthalimide) in its structure [41]. The non-aromatic group was responsible for the first decomposition peak through ether and isopropylene groups scissioning with resulting small amounts of water to hydrolyze the imide groups. These aromatic groups were also presented in the second peak. Lastly, the residual weight percentage at 800 °C under N<sub>2</sub> atmosphere was 52.86% for neat PEI, 55.42% for 1 wt.% CNTs/PEI and 57.14% for 3 wt.% CNTs/PEI.

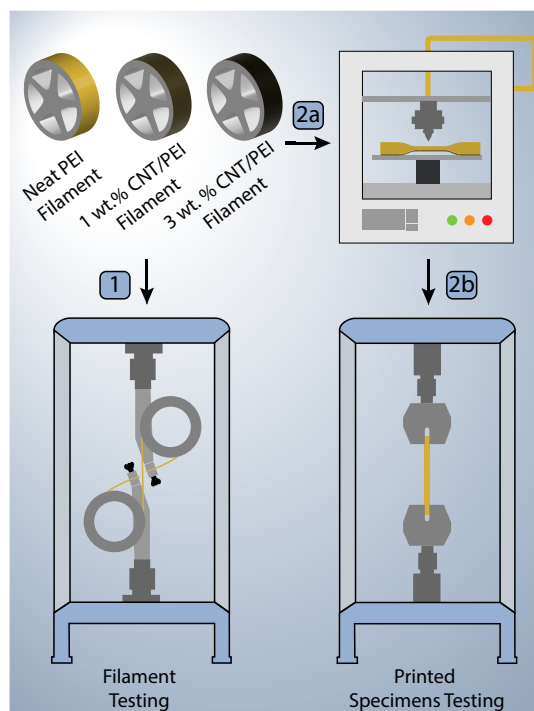


Figure 5: Road map of mechanical characterizations. Route-1 represents the characterization of the feedstock filaments for neat PEI, 1 and 3 wt.% CNTs/PEI; and Route-2 describes the characterization of the additively manufactured specimens after printing (2a) and ASTM 638 and 3039 mechanical tensile tests by UTM (2b).

The amount of CNTs resulted in a difference in residues and concluded that adding CNTs increased the thermal stability of PEI.

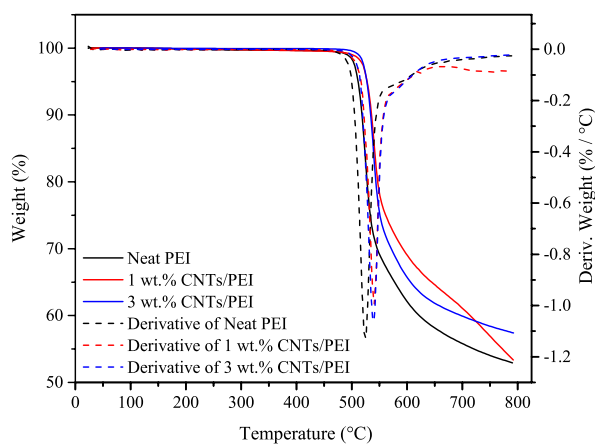


Figure 6: TGA analysis of neat PEI and 1 and 3 wt.% of CNTs/PEI filaments, along with the first derivative of mass change (DTG) in the TGA graph.

Although some of the properties such as printing parameters and processing temperature can be adjusted in FFF, still there is a lack of knowledge on the viscosity and processibility variation when reinforced filaments are considered. For repeatable and good-quality specimens the rheology of neat and CNTs/PEI composites was evaluated to broaden our understanding further. For rheology assessment of melt-processing, the storage ( $G'$ ) and loss moduli ( $G''$ ), the damping factor ( $\tan \delta$ ), and the complex viscosity ( $\eta^*$ ) of neat PEI, 1, and 3 wt.% CNTs/PEI filaments were exhibited

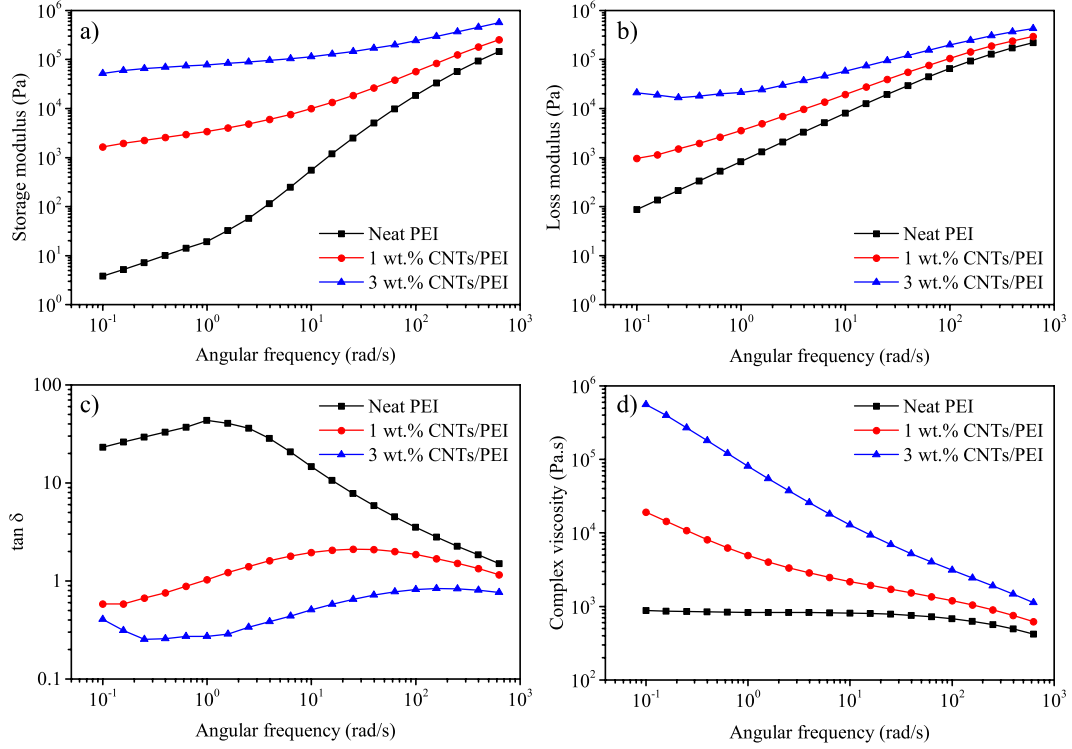


Figure 7: (a) Storage modulus ( $G'$ ), (b) loss modulus ( $G''$ ), (c) damping factor ( $\tan \delta$ ), (d) complex viscosity ( $\eta^*$ ) as a function of frequency for neat PEI, 1 wt.% CNTs/PEI, and 3 wt.% CNTs/PEI filaments.

in Fig. 7 by a function of angular frequency. As typical of most polymer systems, dynamic moduli curves of filaments increase with increasing angular frequency (Fig. 7a,b). Compared to the relaxation time of the polymer chains, the test time is significant at relatively low frequencies, revealing that the chains readily return to their original state. Otherwise, at higher frequencies, the test time is too short of recovering their position and thus, the system exhibits greater stiffness [42].

At viscoelastic theory, the solid (elastic) behavior of the material is represented by storage modulus, whereas the liquid (viscous) behavior of the material is characterized by loss modulus [42]. The ratio of loss modulus to storage modulus expresses the relative stiffness and is mentioned often as the damping factor. The crossover point ( $G''/G' = 1$  or  $\tan \delta$ ) was only observed on the  $\tan \delta$  curve of 1 wt.% CNTs/PEI filament (Fig. 7c). Before the crossover point ( $\omega < \sim 1$  rad/s), the reinforced composite showed an elastic behavior, while after this point, it presented viscous behavior ( $\omega > \sim 1$  rad/s). On the other hand, neat PEI presented primarily viscous behavior with storage modulus curve placed underneath the loss modulus curve ( $\tan \delta$  values rated over 1), and 3 wt.% CNTs/PEI filament oppositely shows primarily elastic behavior with  $\tan \delta$  curve values between 0 and 1 (Fig. 7c) presenting enhanced stiffness characteristics in line with the mechanical characterizations.

The complex viscosity curves of all filaments have shown frequency-dependent shear-thinning behavior (Fig. 7d). However, the neat PEI filament shows a Newtonian behavior at low frequencies before exhibiting shear-thinning behavior at angular frequencies greater than 100 rad/s. The power-law model describes the shear thinning behavior as

$$\eta = k(\dot{\gamma})^{n-1} \quad (1)$$

where  $\eta$  is the shear viscosity,  $\dot{\gamma}$  is the shear rate,  $k$  is the consistency index, and  $n$  is the power-law index [43]. By considering the Cox-Merz rule [ $\eta(\dot{\gamma}) = \eta(\omega)$  for  $\dot{\gamma} = \omega$ ], the shear-thinning exponent,  $n$ , was calculated as 0.75, 0.54, and 0.28 for neat PEI, 1, and 3 wt.% CNTs/PEI filaments, respectively. It is clear that the amount of shear-thinning was raised by the addition of CNTs; in other words, lower  $n$  values were observed with increasing filler loading as

expected [43, 44]. Finally, it must be considered that adequate driving pressure was needed in the extruder of the FFF system to overcome a high shear viscosity of CNTs/PEI filament which also should be considered for large-scale additive manufacturing studies within these reinforced PEI filaments.

The electrical conductivities of fabricated filaments were listed in Table 1 with the weight and volume percentage of CNTs reinforcements. The weight fractions, wt.%, were converted to volume fractions, vol.%, based on a theoretical density of 1.8 g/cm<sup>3</sup> [45]. Based on the conductivity value of neat PEI ( $10^{-15}$  S/cm) and the previous study [7], it is clear that both CNTs/PEI filaments were beyond the percolation threshold of their system.

Table 1: Electrical conductivities of CNTs/PEI filaments.

CNTs wt.%	CNTs vol.%	Conductivity (S/cm)
0	0	$10^{-15}$
1	0.71	$2.93 \times 10^{-3}$
3	2.14	$1.07 \times 10^{-2}$

The lower percolation threshold is primarily driven through the physical geometries of fillers as CNTs used in here and their homogenous and uniform dispersion in the polymer matrix [45–47]. When compared between many dispersion methods such as melt mixing or sonication, the percolation threshold was achieved at lower weight fractions with a more efficient mechanism to force the distribution and dispersion of the fillers in sonication [10, 48–50]. However, extrusion of polymers as an industrially compatible method is more prevalent in mass production [43, 51, 52]. Pötschke et al. have presented that the separation distance between CNTs was relatively short in the PEI matrix, also showing due to the amorphous nature of the chain without any crystalline sites to disturb and finally resulting in an increase in the conductivity.

Since the CNTs inclusion in the PEI matrix may significantly change polymer chain conformality and entanglement characteristics, mechanical properties were evaluated by tensile testing of neat and CNTs/PEI composite filaments as presented in Fig. 8a. The representative stress-strain curves for the feedstock filaments of PEI and CNTs/PEI are shown in Fig. 8b. Mean values of UTS were calculated as  $99.62 \pm 0.84$  MPa,  $100.39 \pm 1.03$  MPa, and  $104.26 \pm 1.77$  MPa for neat PEI, 1 wt.% CNTs/PEI, and 3 wt.% CNTs/PEI, respectively. The mechanical behavior of the fabricated neat PEI filament was in line with the values provided by the leading material supplier Sabic [53]. The results pointed out that, the UTS of 1 wt.% CNTs/PEI and neat PEI were similar, whereas the enhancement obtained by 3 wt.% CNTs was approximately 5%. Earlier studies, primarily involving moderate thermoplastics such as PLA or ABS, reported up to a 60% increase in tensile strength due to deficient strength polymer reinforcement mechanisms observed when a high aspect ratio and stiff filler such as CNTs were added [8, 37, 54]. However, similar to the present study, the mechanical properties of high-performance thermoplastics which exhibit a strength much higher than those of commodity ones, were slightly increased [11, 52].

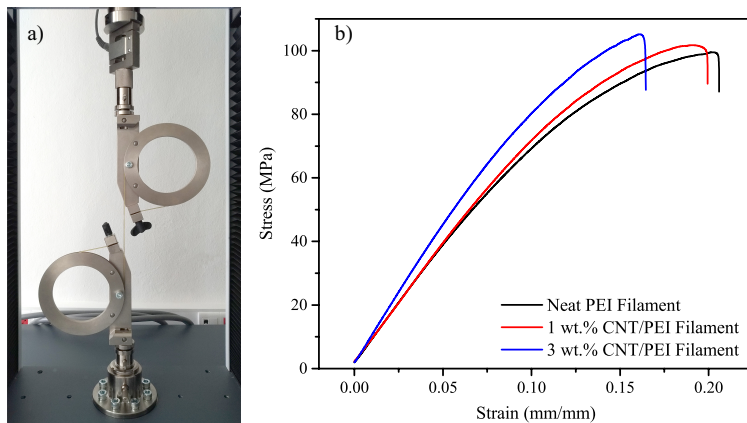


Figure 8: (a) Tensile test of feedstock filaments with capstan grips, (b) representative stress-strain graph of neat PEI, 1 wt.% CNTs/PEI, and 3 wt.% CNTs/PEI filaments.

Moreover, these results articulate that in a matrix-filler system, filler materials tend to limit the strain of polymers by concentrating the load on themselves due to their higher elastic moduli increasing the UTS of the polymer [4, 55–57]. However, CNTs do not interact similarly with both semi-crystalline and amorphous polymers. For the semi-crystalline polymers, CNTs in the matrix act as “nucleating sites,” inducing crystallization. Thus, CNTs enhance the semi-crystalline polymers by increasing the crystallization and intrinsic tensile properties [58]. On the other hand, for amorphous polymers, no crystallization occurs, and CNTs increase their mechanical properties by limiting the mobility of the polymer chains and carrying the load by themselves in their vicinity by  $\pi$ -interactions [7].

Due to strong Van der Waals interactions, CNTs are prone to agglomerate, thus leading to inhomogeneity of the composites [59]. This could lead to highly inconsistent mechanical properties. However, the standard deviations and the values of UTS of the specimens showed that the fabricated composites did not contain any significant agglomeration. This result can be associated with the composites cycling in the melt extrusion system 5 times, resulting in a decrease in CNTs length and potentially molecular weight of neat PEI [36, 60]. Remarkably when the CNTs were reached to 3 wt.% in PEI, the elongation at break % was dropped compared to neat and 1 wt. % CNTs/PEI composites attributed to the trade-off between CNTs addition and introducing brittleness arising in the nature of PEI matrix. Still, the elasticity is comparable with the reinforced polymer matrices for an FFF system as clearly presented in this study.

In earlier studies, it was attributed that a consistent  $T_g$  range brings practical advantages for 3D printing applications [7]. However, keeping the balance between multifunctionality created by CNTs and a high-performance polymer and printing system usually brings additional challenges. In this study, optimizing printing temperature depending on the variation in reinforced polymer viscosity is a one-step challenge that needs to be addressed. Hence, empirical studies are performed for defining these conditions here.

A thermoplastic polymer as a shear-thinning fluid obeys Hagen-Poiseuille law while flowing in the nozzle, which can be described as a pipe with a narrow radius. Therefore, the fluid velocity reaches its maximum value at the center of the nozzle; however, the velocity drops to zero at the nozzle wall (Fig. 9a). This parabolic shaped fluid velocity behavior depending on the radius of the nozzle can be expressed as,

$$u(r) = \frac{3n + 1}{n + 1} \bar{V} \left[ 1 - \left( \frac{r}{R} \right)^{\frac{1+n}{n}} \right] \quad (2)$$

and the shear rate calculated by the velocity is

$$\dot{\gamma} = \frac{du}{dr} = \frac{3n + 1}{nR} \bar{V} \left[ \left( \frac{r}{R} \right)^{\frac{1+n}{n} - 1} \right] \quad (3)$$

where,  $\bar{V}$  is the average inlet velocity of the polymer,  $r$  is the distance from the center of the nozzle,  $R$  is the nozzle radius, and  $n$  is the power index [61].

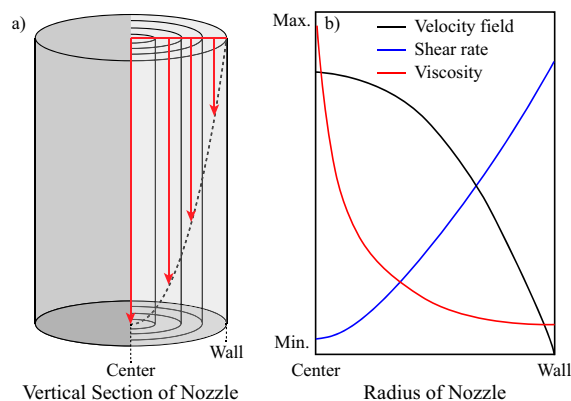


Figure 9: (a) Velocity differences of the fluid from the wall to the center of the nozzle, and (b) representative curves for the velocity field, shear rate, and viscosity along the radius of the nozzle. Red arrows illustrating the velocity vectors in different layers.

According to Eq. 3, the shear rate on the polymer attains its maximum value at the nozzle wall, which is inversely proportional to the velocity; hence the shear rate is not constant over the cross-section of the nozzle. As the most important result, the molten filament's viscosity varies along the radius to the shear rate due to the shear-thinning. In summary, Fig. 9b represents the velocity field, shear rate, and viscosity variations corresponding to the distance from the nozzle's wall or center.

Alongside, the viscosity behavior of the relevant filament could be a guide for choosing the proper print or liquefier temperature in a condition where the nozzle diameter and inlet velocity are constant. At high temperatures, the high fluidity of the molten thermoplastic determines the consistency of the printing process. The polymer chains require higher mobility to diffuse and form entanglements. The lower viscosity ensures these obligations, particularly for the merge of the extrudates. In addition, the difference in viscosity along the nozzle radius mentioned above also affects the profile of the extrudate in a way that causes issues such as the shark-skin effect. One earlier study showed that the gap between maximum and minimum viscosity values along the nozzle radius decreased at higher temperatures [61].

Nevertheless, excessive temperature yields low precision through the printing process and fabricates flawed objects exhibiting holes and surface roughness. This phenomenon defines an upper limit on increasing the temperature. Therefore, the print temperature should be chosen such that it is neither insufficient to reduce the viscosity difference on flow cross-section and low enough to weaken the flow nor high enough to reduce the printing quality.

In this study, print temperatures for each feedstock filament of neat PEI and CNTs/PEI by the principle mentioned above with empirical observations. Six different candidate temperatures ranging from 360 °C to 390 °C were determined based on the extruder's die zone (or nozzle) temperature during the filaments' manufacturing (Fig. 1a). Two different samples prepared by each fabricated feedstock filament were examined using an optical microscope. Microfilaments called extrudates are extruded from the nozzle of the 3D printer, and the single layers were deposited on the bed of the 3D printer. All neat PEI samples were illuminated below; however, CNTs/PEI filaments were imaged with the light source from the top. All microscope images were added in the supplementary material.



Figure 10: Microscope images of single layer printing and extrudates by neat PEI, 1 wt.% CNTs/PEI, and 3 wt.% CNTs/PEI filaments. Each row represents the corresponding filament with the name written in the upper left presenting different printing temperatures.

Extrudates of neat PEI exhibited a stable behavior without any deformation and air bubbles until 380 °C, and the contour distortions of the extrudates began to be observed at temperatures higher than 380 °C (Fig. S1). On the other hand, the printing quality of the single layers of neat PEI at different temperatures was similar to that of the extrudates

(Fig. S2). The tearing between the deposited lines, which can be associated with the highly viscous nature of the polymer, was not observed in any single layer printed by a neat PEI filament. However, at higher temperatures than 375 °C, the deposited lines were intricate, while the contour sharpness of the layer disappeared. Therefore, 375 °C was chosen for printing or liquefier temperatures of neat PEI filament.

Significant deformation was not observed in the extrudates of both CNTs/PEI filaments at any specified temperature. However, microscope pictures of single layers were more pronounced to understand the printing characteristic of CNTs/PEI filaments with their associated temperatures. For 1 wt.% CNTs/PEI filament, the intersection between the deposited lines became more distinct due to the shrinkage of each line correlated to higher viscosity, at temperatures up to 380 °C (Fig. S4). This effect is so strong that it led to tearing at the intersection of deposited lines for 3 wt.% CNTs/PEI filament at relatively low temperatures (Fig. S6). Considering the deformities at 390 °C (Fig. 10e,h) and the issues discussed at low temperatures for CNTs/PEI filaments, 380 °C was selected for 1 wt.% CNTs/PEI (Fig. 10d) and 385 °C for 3 wt.% CNTs/PEI filament (Fig. 10g).

Lastly, although rheological results (obtained at 360 °C, Fig. 7) showed that the print temperature of the CNTs/PEI filaments could be increased due to the viscosity differences between the neat and the reinforced PEIs, it would not be incorrect to claim that the difference between the print temperatures of feedstock filaments must be low for a reasonable comparison of the mechanical properties. In conclusion, the print temperatures were chosen with an increase of 5 °C from the neat PEI to 3 wt.% CNTs/PEI.

As indicated by Ahn *et al.* [30], unavoidable porosity occurred in the neck/curved region of the ASTM D638 samples. Fig. 11 shows the single layer images of the ASTM D638 and D3039 samples both in *Rectilinear* and *Concentric* patterns. In both images, voids were distinct due to the characteristic motion of FFF/3D printers with linear motion conveying belts. Thus, circular sections on a layer cannot be filled. Furthermore, regular void formations were observed on the gage section of ASTM D638 and D3039 *Rectilinear* specimens. In addition, the void density at the gage section of ASTM D638 specimens was higher than of the ASTM D3039 specimens, resulting in a more unpredictable mechanical behavior. No voids were observed in the gage section of ASTM D638 *Concentric* specimens. However, a more considerable void was detected in the middle of the radiused section due to the printing pattern, leading to inconsistent mechanical results due to stress concentration around that specific region.

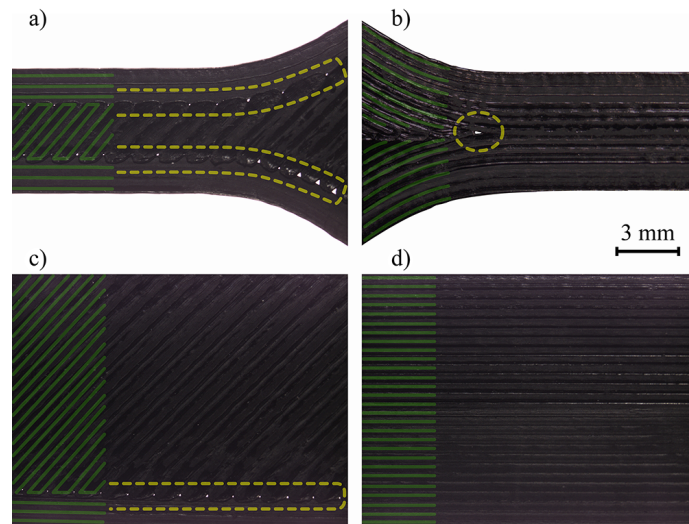


Figure 11: Single layer microscope images showing four distinct specimens and printing patterns (green lines) and void concentration zones (yellow dashed lines). (a) belongs to ASTM D638 *Rectilinear* while (b) ASTM D638 *Concentric*, (c) ASTM D3039 *Rectilinear*, and (d) ASTM D3039 *Concentric*.

On the other hand, ASTM D3039 *Concentric* specimens did not contain any voids outside the gripping sections. Since voids in the printed sample cause early failure and that specimens manufactured by FFF are not identical, all of them are unique [62]. It is usually inadequate to make comparisons in a unified approach with unpredictable mechanical behavior. However, creating big data pools for FFF manufactured parts for mechanical testing can lead to

a more conclusive finding through validation by the standard deviation of mechanical tests.

The mean UTS values and corresponding standard deviation values are as shown in Fig. 12. 1 wt.% and 3 wt.% CNTs reinforced specimens are named under their loading rates, where unreinforced specimens are named neat.

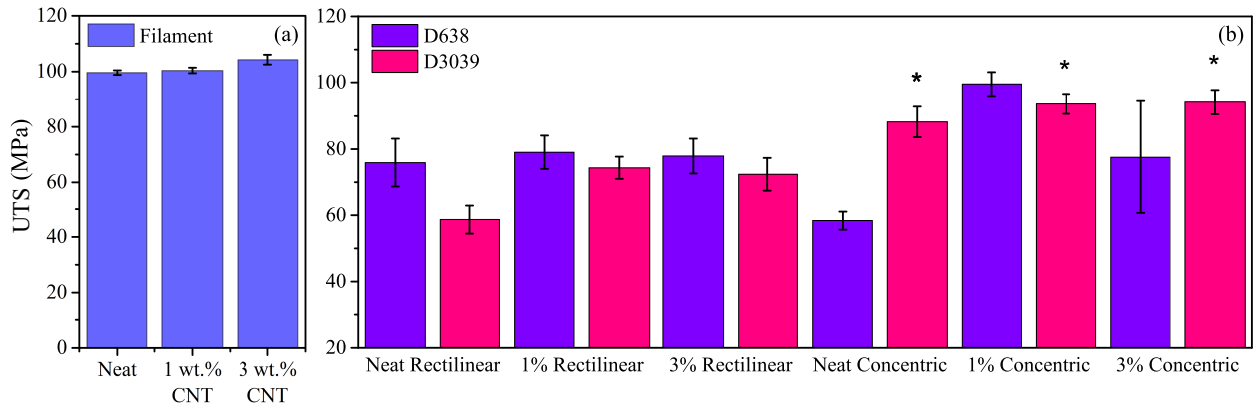


Figure 12: Mechanical results of (a) filaments and (b) FFF printed specimens.

Fig. 12 indicates that specimens produced by depositing the filament along the tensile stress direction showed better tensile performance than those of the *Rectilinear* pattern, as expected. The only result that conflicts with this observation is Neat *Concentric* of D638, which yielded a lower tensile strength than Neat *Rectilinear* of D638. When comparing the D638 and D3039 specimens on individual printing patterns, for *Rectilinear*, misleading information that D638 specimens fit better with the trend of the materials in filament form can be obtained. However, it should be underlined that UTS values of the aforementioned specimens have a higher standard deviation than that of the D3039 specimens, as pointed out while conducting the single layer microscopy characterization. On the other hand, for *Concentric* pattern samples, UTS of the D638 specimens have shown remarkably inconsistent results. This can be explained by the unfilled area presented in the center of the curved region, as seen in Fig. 11. As mentioned before, filling a curved area with only linear motion is impractical. Nevertheless, ASTM D3039 *Concentric* samples showed outstanding fit with the trend of the filaments in composite forms for strength evaluation. Further, the aforementioned samples have the lowest overall standard deviations among all subgroups, as expected by the single-layer microscopy characterization. The lower standard deviation of UTS of ASTM D3039 samples has indicated that this test standard can yield more reliable mechanical results than ASTM D638. In particular, ASTM D3039 *Concentric* specimens performed best, providing the lowest overall standard deviation, highest overall UTS, and best fitting with the mechanical character of reinforced filament. Further relevant statistical calculations relating the Linear Correlation Coefficients and Confidence Intervals of all data sets for 90% can be found on the supplementary material.

Based on the ASTM D3039, tensile failure modes of all specimens were determined, whether they are prepared in corresponding geometry or ASTM D638. Before adopting this notation, it should be noted that despite the similarity in terms of layered nature between FFF and laminated structures, it was observed that FFF tensile specimens tend to fail at multiple areas and various locations than classical laminated composites do. Table 2 shows the failure modes of the tensile specimens, from most to least frequent. This classification was executed only for individual specimen geometries and printing patterns, including all neat PEI, 1 wt.%, and 3 wt.% CNTs/PEI in their corresponding specimen geometries and printing patterns since no distinct fracture modes are observed depending on aforementioned materials. It is also proper to mention that character “R”, which describes the failures at the radiused region of the D638 specimens, is added to this notation in this paper. Although this fracture type can be expressed as “Other”, which stands in the ASTM D3039 notation, it needs to be described by its character for the sake of clarity. Representative images of fracture types that are tabulated in Table 2 are given in Fig S7.

As mentioned above, FFF specimens mainly failed in multiple areas. For ASTM D3039 specimens, fractures both at the gripping section and gage section were observed for most of the specimens. Due to that, it is not much possible to detect the early failures with failure modes. Overall, either *Rectilinear* or *Concentric* the tests performed under ASTM D638 standard presents fracture modes with “R” as their second character, such as LRT and LRV, dominantly. Large majority of ASTM D3039 *Rectilinear* specimens have presented LGV fracture modes. Due to the

Table 2: Fracture modes observed for each specimen geometry and pattern type tested by ASTM D638 and ASTM 3039 for neat PEI and 1% and 3% CNTs/PEI. The data pool is only specifically listed for their pattern of printing.

Sample	Fracture Mode*
<i>Rectilinear</i> ASTM D638	LRT, LGM
<i>Rectilinear</i> ASTM D3039	LGV
<i>Concentric</i> ASTM D638	LRT, LRV
<i>Concentric</i> ASTM D3039	LAT, SMV

\*First characters: L: Lateral, S: Long, splitting

Second characters: R: radius (defined for FFF), G: gage, M: multiple areas, A: At grip/tab

Third characters: T: top, M: middle, V: various

brittle behavior of FFF specimens, the specimens failed at various locations, yet failures at the gage section were also observed. For ASTM D638 *Concentric* specimens, very few specimens showed a fracture at the gage section. The remainder of the specimens fractured at the radiused section was not acceptable by the ASTM D638 failure criteria. For ASTM D638 *Rectilinear* specimens, fractures at the gage section were observed more than those of *Concentric* specimens. However, failures at the radiused section were still observed frequently. Furthermore, a significant portion of the specimens has shown lateral fracture type rather than angled. This result was reasonable regarding that the specimens had no long fibers to hold the vicinity of the initial cracks that arose in the matrix as laminated structures offer.

#### 4. Conclusion

In this research, mechanical properties of CNTs reinforced PEI filaments and printed coupon specimens were studied as a function of CNTs concentration for 1 and 3 wt.% fabricated by melt processing. Several printing temperatures and orientations were analyzed to reveal the effect of CNTs addition to a high-performance polymer for mechanical characterizations. The thermal stability of neat and CNTs reinforced PEI presented an increase from 524 °C to 539 °C and 537 °C for neat, 1, and 3 wt.% CNTs, respectively. Notably, since the rheology of PEI is crucial to understanding the effect of CNTs and efficient printability, the rheological analysis has been performed. Therefore, a shear-thinning behavior was observed with increasing CNTs content corresponding to a decreased shear-thinning exponent  $n$  as 0.75, 0.54, and 0.28 for neat PEI, 1, and 3 wt.% CNTs/PEI filaments, respectively. Within the viscosity differences for neat and CNTs reinforced PEI, printing temperatures were optimized by exploring the single layer printing and extrudates. It was concluded that the reinforced CNTs were effectively printed when the nozzle temperature was higher than neat PEI. Numerically, it is found that increasing the nozzle temperature by 5 °C compared to neat PEI yields better results in terms of printing quality while printing %1 CNTs/PEI. Similarly, a 10 °C temperature rise is necessary for printing quality for 3 wt.% CNTs/PEI. As with typical FFF printed parts, void formation is an essential aspect of the mechanical properties. Basic infill patterns of *Rectilinear* and *Concentric* with 3 outer shells and 100% infill rate were printed as the two most widely explored raster orientations. Furthermore, the printed specimens were both tested with ASTM D3039 and ASTM D638 for a deep understanding of the differences that may emerge from testing protocol differences. The void density at the gage section of ASTM D638 specimens was higher than of the ASTM D3039 specimens, resulting in a more unpredictable mechanical behavior. Overall for the tensile testing of printed parts, CNTs and PEI followed similar trends of filament testing with the increase in strength for specimens tested with ASTM D3039. Along with the results of the materials of the filament form, this result implies two conclusions; first, introducing CNTs in the PEI matrix have increased the mechanical properties of the material, second, FFF processing parameters for 3 wt.% CNTs/PEI were not fully optimized, thus leading defects in the specimen, which additive manufacturing is prone to. ASTM D3039 *Concentric* specimens performed best by providing the lowest overall standard deviation, highest overall UTS, and best fitting with the mechanical character of reinforced filament. The results presented failures mostly in multiple areas for failure modes of ASTM D638 and ASTM D3039 tested FFF specimens. Although ASTM D638 failure types dominated at the angled radius/curved region leading to an unsuccessful testing process, ASTM D3039 presented lateral gage region dominated multiple areas failures representing the capability with the low standard deviation in strength.

## 5. Acknowledgment

This work was financially supported by Boeing Global Co. with project number 2016000269. The authors are grateful to Dyze Design for providing technical support. The authors would also like to thank Suat Ebil for contributing to extrusion process and Yunus Emre Bozkurt for conducting rheological characterizations.

## References

### References

- [1] Y. Yan, S. Li, R. Zhang, F. Lin, R. Wu, Q. Lu, Z. Xiong, X. Wang, Rapid prototyping and manufacturing technology: principle, representative technics, applications, and development trends, *Tsinghua Science and Technology* 14 (S1) (2009) 1–12.
- [2] H. Wu, M. Sulkis, J. Driver, A. Saade-Castillo, A. Thompson, J. H. Koo, Multi-functional ultem™ 1010 composite filaments for additive manufacturing using fused filament fabrication (fff), *Additive Manufacturing* 24 (2018) 298–306.
- [3] R. Zaldivar, T. Mclouth, G. Ferrelli, D. Patel, A. Hopkins, D. Witkin, Effect of initial filament moisture content on the microstructure and mechanical performance of ultem® 9085 3d printed parts, *Additive Manufacturing* 24 (2018) 457–466.
- [4] A. C. de Leon, Q. Chen, N. B. Palaganas, J. O. Palaganas, J. Manapat, R. C. Advincula, High performance polymer nanocomposites for additive manufacturing applications, *Reactive and Functional Polymers* 103 (2016) 141–155.
- [5] M. Arif, H. Alhashmi, K. Varadarajan, J. H. Koo, A. Hart, S. Kumar, Multifunctional performance of carbon nanotubes and graphene nanoplatelets reinforced peek composites enabled via fff additive manufacturing, *Composites Part B: Engineering* 184 (2020) 107625.
- [6] J. C. Najmon, S. Raeisi, A. Tovar, Review of additive manufacturing technologies and applications in the aerospace industry, *Additive manufacturing for the aerospace industry* (2019) 7–31.
- [7] O. Kaynan, A. Yildiz, Y. E. Bozkurt, E. O. Yenigun, H. Cebeci, Electrically conductive high-performance thermoplastic filaments for fused filament fabrication, *Composite Structures* 237 (2020) 111930.
- [8] L. Yang, S. Li, X. Zhou, J. Liu, Y. Li, M. Yang, Q. Yuan, W. Zhang, Effects of carbon nanotube on the thermal, mechanical, and electrical properties of pla/cnt printed parts in the fdm process, *Synthetic Metals* 253 (2019) 122–130.
- [9] E. J. Siochi, D. C. Working, C. Park, P. T. Lillehei, J. H. Rouse, C. C. Topping, A. R. Bhattacharyya, S. Kumar, Melt processing of swcnt-polyimide nanocomposite fibers, *Composites Part B: Engineering* 35 (5) (2004) 439–446.
- [10] K. Gnanasekaran, T. Heijmans, S. Van Bennekom, H. Woldhuis, S. Wijnia, G. De With, H. Friedrich, 3d printing of cnt-and graphene-based conductive polymer nanocomposites by fused deposition modeling, *Applied materials today* 9 (2017) 21–28.
- [11] S. Berretta, R. Davies, Y. Shyng, Y. Wang, O. Ghita, Fused deposition modelling of high temperature polymers: Exploring cnt peek composites, *Polymer Testing* 63 (2017) 251–262.
- [12] J. M. Gardner, G. Sauti, J.-W. Kim, R. J. Cano, R. A. Wincheski, C. J. Stelter, B. W. Grimsley, D. C. Working, E. J. Siochi, Additive manufacturing of multifunctional components using high density carbon nanotube yarn filaments, *NASA Langley Research Center: Hampton, VA, USA*.
- [13] S. Lebedev, O. Gefle, E. Amitov, D. Y. Berchuk, D. Zhuravlev, Poly (lactic acid)-based polymer composites with high electric and thermal conductivity and their characterization, *Polymer Testing* 58 (2017) 241–248.
- [14] A. Dorigato, V. Moretti, S. Dul, S. Unterberger, A. Pegoretti, Electrically conductive nanocomposites for fused deposition modelling, *Synthetic Metals* 226 (2017) 7–14.
- [15] A. Mora, P. Verma, S. Kumar, Electrical conductivity of cnt/polymer composites: 3d printing, measurements and modeling, *Composites Part B: Engineering* 183 (2020) 107600.
- [16] L. Han, Q. Song, J. Sun, K. Li, Y. Lu, The role of cnt in improving the mechanical strength retention rate of c/c composites during heat treatment, *Composites Part B: Engineering* 187 (2020) 107856.
- [17] J. R. C. Dizon, A. H. Espera Jr, Q. Chen, R. C. Advincula, Mechanical characterization of 3d-printed polymers, *Additive Manufacturing* 20 (2018) 44–67.
- [18] K. C. Chuang, J. E. Grady, R. D. Draper, E.-S. E. Shin, C. Patterson, T. D. Santelle, Additive manufacturing and characterization of ultem polymers and composites, in: *Proceedings of the CAMX Conference, Dallas, TX, USA, 2015*, pp. 26–29.
- [19] J. Chacón, M. Caminero, P. Núñez, E. García-Plaza, I. García-Moreno, J. Reverte, Additive manufacturing of continuous fibre reinforced thermoplastic composites using fused deposition modelling: Effect of process parameters on mechanical properties, *Composites science and technology* 181 (2019) 107688.
- [20] M. Á. Caminero, J. M. Chacón, E. García-Plaza, P. J. Núñez, J. M. Reverte, J. P. Becar, Additive manufacturing of pla-based composites using fused filament fabrication: Effect of graphene nanoplatelet reinforcement on mechanical properties, dimensional accuracy and texture, *Polymers* 11 (5) (2019) 799.
- [21] B. Rankouhi, S. Javadpour, F. Delfanian, T. Letcher, Failure analysis and mechanical characterization of 3d printed abs with respect to layer thickness and orientation, *Journal of Failure Analysis and Prevention* 16 (3) (2016) 467–481.
- [22] C. Hohimer, N. Aliheidari, C. Mo, A. Ameli, Mechanical behavior of 3d printed multiwalled carbon nanotube/thermoplastic polyurethane nanocomposites, in: *Smart Materials, Adaptive Structures and Intelligent Systems, Vol. 58257, American Society of Mechanical Engineers, 2017*, p. V001T08A004.
- [23] H. R. Dana, F. Barbe, L. Delbreilh, M. B. Azzouna, A. Guillet, T. Breteau, Polymer additive manufacturing of abs structure: Influence of printing direction on mechanical properties, *Journal of Manufacturing Processes* 44 (2019) 288–298.
- [24] G. C. Onwubolu, F. Rayegani, Characterization and optimization of mechanical properties of abs parts manufactured by the fused deposition modelling process, *International Journal of Manufacturing Engineering* 2014.

- [25] M. Iragi, C. Pascual-González, A. Esnaola, C. Lopes, L. Aretxabaleta, Ply and interlaminar behaviours of 3d printed continuous carbon fibre-reinforced thermoplastic laminates; effects of processing conditions and microstructure, *Additive Manufacturing* 30 (2019) 100884.
- [26] L. Safai, J. S. Cuellar, G. Smit, A. A. Zadpoor, A review of the fatigue behavior of 3d printed polymers, *Additive manufacturing* 28 (2019) 87–97.
- [27] A. Pastrnak, A. Henriquez, V. La Saponara, Parametric study for tensile properties of molded high-density polyethylene for applications in additive manufacturing and sustainable designs, *Journal of Applied Polymer Science* 137 (42) (2020) 49283.
- [28] T. J. Gordelier, P. R. Thies, L. Turner, L. Johanning, Optimising the fdm additive manufacturing process to achieve maximum tensile strength: a state-of-the-art review, *Rapid Prototyping Journal*.
- [29] A. Miller, C. Brown, G. Warner, Guidance on the use of existing astm polymer testing standards for abs parts fabricated using fff, *Smart and Sustainable Manufacturing Systems* 3 (1).
- [30] S.-H. Ahn, M. Montero, D. Odell, S. Roundy, P. K. Wright, Anisotropic material properties of fused deposition modeling abs, *Rapid prototyping journal*.
- [31] M. Somireddy, C. Singh, A. Czekanski, Analysis of the material behavior of 3d printed laminates via fff, *Experimental Mechanics* 59 (6) (2019) 871–881.
- [32] K. Saeed, A. McIlhagger, E. Harkin-Jones, J. Kelly, E. Archer, Predication of the in-plane mechanical properties of continuous carbon fibre reinforced 3d printed polymer composites using classical laminated-plate theory, *Composite Structures* 259 (2021) 113226.
- [33] L. Pyl, K.-A. Kalteremidou, D. Van Hemelrijck, Exploration of specimen geometry and tab configuration for tensile testing exploiting the potential of 3d printing freeform shape continuous carbon fibre-reinforced nylon matrix composites, *Polymer Testing* 71 (2018) 318–328.
- [34] R. Zaldivar, D. Witkin, T. McLouth, D. Patel, K. Schmitt, J. Nokes, Influence of processing and orientation print effects on the mechanical and thermal behavior of 3d-printed ultem® 9085 material, *Additive Manufacturing* 13 (2017) 71–80.
- [35] R. Kay, Effect of raster orientation on the structural properties of components fabricated by fused deposition modeling, Ph.D. thesis, The Ohio State University (2014).
- [36] A. Das, C. A. Chatham, J. J. Fallon, C. E. Zawaski, E. L. Gilmer, C. B. Williams, M. J. Bortner, Current understanding and challenges in high temperature additive manufacturing of engineering thermoplastic polymers, *Additive Manufacturing* 34 (2020) 101218.
- [37] N. Van de Werken, H. Tekinalp, P. Khanbolouki, S. Ozcan, A. Williams, M. Tehrani, Additively manufactured carbon fiber-reinforced composites: State of the art and perspective, *Additive Manufacturing* 31 (2020) 100962.
- [38] V. Kishore, C. Ajinjeru, A. Nycz, B. Post, J. Lindahl, V. Kunc, C. Duty, Infrared preheating to improve interlayer strength of big area additive manufacturing (baam) components, *Additive Manufacturing* 14 (2017) 7–12.
- [39] I. Miccoli, F. Edler, H. Pfnür, C. Tegenkamp, The 100th anniversary of the four-point probe technique: the role of probe geometries in isotropic and anisotropic systems, *Journal of Physics: Condensed Matter* 27 (22) (2015) 223201.
- [40] L. Santos, B. Ribeiro, L. Hein, E. Botelho, M. Costa, Processing, thermal and mechanical behaviour of pei/mwcnt/carbon fiber nanostructured laminate, *Materials Research Express* 4 (11) (2017) 115037.
- [41] S. Carroccio, C. Puglisi, G. Montaudo, Thermal degradation mechanisms of polyetherimide investigated by direct pyrolysis mass spectrometry, *Macromolecular Chemistry and Physics* 200 (10) (1999) 2345–2355.
- [42] R. Guo, J. Azaiez, C. Bellehumeur, Rheology of fiber filled polymer melts: Role of fiber-fiber interactions and polymer-fiber coupling, *Polymer Engineering & Science* 45 (3) (2005) 385–399.
- [43] P. Pötschke, T. Fornes, D. Paul, Rheological behavior of multiwalled carbon nanotube/polycarbonate composites, *Polymer* 43 (11) (2002) 3247–3255.
- [44] V. Kishore, C. Ajinjeru, A. A. Hassen, J. Lindahl, V. Kunc, C. Duty, Rheological behavior of neat and carbon fiber-reinforced poly (ether ketone ketone) for extrusion deposition additive manufacturing, *Polymer Engineering & Science* 60 (5) (2020) 1066–1075.
- [45] J. Li, P. C. Ma, W. S. Chow, C. K. To, B. Z. Tang, J.-K. Kim, Correlations between percolation threshold, dispersion state, and aspect ratio of carbon nanotubes, *Advanced Functional Materials* 17 (16) (2007) 3207–3215.
- [46] G. Pike, C. Seager, Percolation and conductivity: A computer study. i, *Physical Review B* 10 (4) (1974) 1421.
- [47] C. Seager, G. Pike, Percolation and conductivity: A computer study. ii, *Physical Review B* 10 (4) (1974) 1435.
- [48] H. Kim, Y. Miura, C. W. Macosko, Graphene/polyurethane nanocomposites for improved gas barrier and electrical conductivity, *Chemistry of materials* 22 (11) (2010) 3441–3450.
- [49] A.-F. A. Trompeta, E. P. Koumoulos, S. G. Stavropoulos, T. G. Velmachos, G. C. Psarras, C. A. Charitidis, Assessing the critical multifunctionality threshold for optimal electrical, thermal, and nanomechanical properties of carbon nanotubes/epoxy nanocomposites for aerospace applications, *Aerospace* 6 (1) (2019) 7.
- [50] G. Postiglione, G. Natale, G. Griffini, M. Levi, S. Turri, Conductive 3d microstructures by direct 3d printing of polymer/carbon nanotube nanocomposites via liquid deposition modeling, *Composites Part A: Applied Science and Manufacturing* 76 (2015) 110–114.
- [51] R. Zhang, A. Dowden, H. Deng, M. Baxendale, T. Peijs, Conductive network formation in the melt of carbon nanotube/thermoplastic polyurethane composite, *Composites Science and Technology* 69 (10) (2009) 1499–1504.
- [52] A. Isayev, R. Kumar, T. M. Lewis, Ultrasound assisted twin screw extrusion of polymer–nanocomposites containing carbon nanotubes, *Polymer* 50 (1) (2009) 250–260.
- [53] Ultem™resin 1010 global technical data sheet, [https://www.sabic.com/en/products/documents/ultem-resin\\_1010\\_global\\_technical\\_data\\_sheet/en](https://www.sabic.com/en/products/documents/ultem-resin_1010_global_technical_data_sheet/en), accessed: November 2021.
- [54] H. L. Tekinalp, V. Kunc, G. M. Velez-Garcia, C. E. Duty, L. J. Love, A. K. Naskar, C. A. Blue, S. Ozcan, Highly oriented carbon fiber–polymer composites via additive manufacturing, *Composites Science and Technology* 105 (2014) 144–150.
- [55] H. Cebeci, R. G. de Villoria, A. J. Hart, B. L. Wardle, Multifunctional properties of high volume fraction aligned carbon nanotube polymer composites with controlled morphology, *Composites Science and Technology* 69 (15-16) (2009) 2649–2656.
- [56] H. Mattausch, Properties and applications of nanoclay composites, in: *Polymer Nanoclay Composites*, Elsevier, 2015, pp. 127–155.
- [57] S. Pavlidou, C. Papaspyrides, A review on polymer-layered silicate nanocomposites, *Progress in polymer science* 33 (12) (2008) 1119–1198.
- [58] C. A. Chazot, A. J. Hart, Understanding and control of interactions between carbon nanotubes and polymers for manufacturing of high-performance composite materials, *Composites Science and Technology* 183 (2019) 107795.

- [59] M. K. Pitchan, S. Bhowmik, M. Balachandran, M. Abraham, Effect of surface functionalization on mechanical properties and decomposition kinetics of high performance polyetherimide/mwcnt nano composites, *Composites Part A: Applied Science and Manufacturing* 90 (2016) 147–160.
- [60] O. Kaynan, A. Yildiz, Y. E. Bozkurt, E. Ozden Yenigun, H. Cebeci, Development of multifunctional cnts reinforced pei filaments for fused deposition modeling, in: *AIAA Scitech 2019 Forum*, 2019, p. 0406.
- [61] S. B. Balani, F. Chabert, V. Nassiet, A. Cantarel, Influence of printing parameters on the stability of deposited beads in fused filament fabrication of poly (lactic) acid, *Additive Manufacturing* 25 (2019) 112–121.
- [62] S. P. Regalla, S. S. Karwa, S. Rajesh, P. Shyam, P. N. Shrivastava, Strength and fracture behaviour of polymer matrix composite layered structures made by additive manufacturing, *Materials Today: Proceedings* 28 (2020) 1030–1038.